Report

Current Biology

# Interaction between Autonomous and Microtubule Guidance Systems Controls Cellulose Synthase Trajectories

## Graphical Abstract

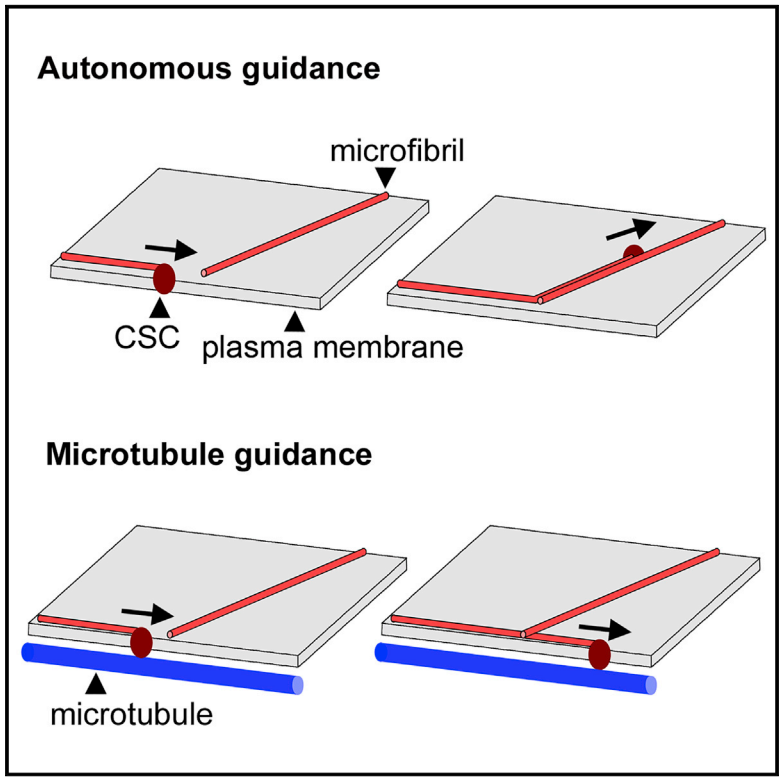


## Highlights

- A dual mechanism guides cellulose synthesis in plant cell walls
- Cellulose synthase complexes autonomously follow trails left by previous complexes
- Microtubule guidance is dominant over autonomous guidance
- Microtubules can guide cellulose synthases directly or indirectly

## Authors

Jordi Chan, Enrico Coen

## Correspondence

jordi.chan@jic.ac.uk (J.C.),
enrico.coen@jic.ac.uk (E.C.)

## In Brief

Chan and Coen reveal a novel mechanism for guiding cellulose synthesizing complexes based on the complexes following trails left by previous complexes. They show that this autonomous mechanism can be overridden by microtubule guidance. This dual guidance system provides a flexible, yet robust control of plant cell wall structure.

Chan & Coen, 2020, Current Biology *30*, 1–7
March 9, 2020 
https://doi.org/10.1016/j.cub.2019.12.066

CellPress

Please cite this article in press as: Chan and Coen, Interaction between Autonomous and Microtubule Guidance Systems Controls Cellulose Synthase Trajectories, Current Biology (2019), https://doi.org/10.1016/j.cub.2019.12.066

Current Biology
Report



# Interaction between Autonomous and Microtubule Guidance Systems Controls Cellulose Synthase Trajectories

Jordi Chan[1,*] and Enrico Coen[1,2,*]
[1]Department of Cell and Developmental Biology, John Innes Centre, Colney Lane, Norwich NR4 7UH, UK
[2]Lead Contact
*Correspondence: jordi.chan@jic.ac.uk (J.C.), enrico.coen@jic.ac.uk (E.C.)
https://doi.org/10.1016/j.cub.2019.12.066

## SUMMARY

**The organization of cellulose microfibrils is critical for the strength and growth of plant cell walls. Microtubules have been shown to play a key role in controlling microfibril organization by guiding cellulose synthase complexes [1–4]. However, cellulose synthase trajectories can be maintained when microtubules are removed by drugs, suggesting a separate guidance mechanism is also at play [1, 5, 6]. By slowing down microtubule dynamics, we reveal such a mechanism by showing that cellulose synthase complexes can interact with the trails left by other complexes, causing them to follow the trails or disappear. The stability of the trails, together with the sensitivity of their directions to cellulase treatment, indicates they most likely reflect nascent cellulose microfibrils. Over many hours, this autonomous mechanism alone can lead to a change in the dominant orientation of cellulose synthase trajectories. However, the mechanism can be overridden by the microtubule guidance system. Our findings suggest a dual guidance model, in which an autonomous system, involving interaction between cellulose synthases and microfibrils, can maintain aligned cellulose synthase trajectories, while a microtubule guidance system allows alignments to be steered by environmental and developmental cues.**

## RESULTS AND DISCUSSION

### Cellulose Synthase Complexes Interact with the Trails Left by Other Complexes

The organization of fibers in the extracellular matrix is critical for the mechanical support and protection of bacterial, plant, and animal cells. These fibers are typically synthesized by complexes at the plasma membrane, but the mechanisms determining the trajectories of these complexes, and thus fiber alignments, are still unclear [7–11].

In plants, cellulose microfibrils are aligned and bundled with other microfibrils in the cell wall to form an interconnected, reticulated network [12, 13]. Micofibrils are generated by cellulose synthase complexes (CSCs) [14, 15]. The trails of nascent cellulose microfibrils are thought to propel the complexes through the plasma membrane, generating streams of CSC particles. Cortical microtubules play a major role in guiding these streams, as CSCs are delivered to, and follow the path of, microtubules [1, 2, 16, 17].

Approximately 40% of CSCs are observed in the gaps between microtubules [18], yet exhibit aligned trajectories [19], raising the question of how they are guided. We refer to these unattached CSCs as autonomous complexes (ACs). It has been proposed ACs are guided by corralling by nearby microtubules [19]. However, ACs continue to display aligned trajectories for hours after removal of microtubules by treatment with oryzalin [1], showing that corralling of ACs is not needed. It is possible that ACs persist in their trajectories after detaching from microtubules [1]. However, given the lifespan of CSCs has been estimated to be ~7 min [20], this mechanism cannot explain how aligned AC trajectories are maintained for hours. Instead, a microtubule-independent alignment mechanism is implicated. Such a mechanism, based on mobile insertion domains, has been proposed for generating helicoidal arrays during secondary thickening [21], but the mechanisms involved in growing plant cells remain unclear.

Here, we use live imaging of developing leaf cells to follow AC dynamics. Because of the high density of microtubules, following the behavior of ACs is technically challenging. We therefore sought to introduce wider gaps between microtubules by exposing leaves to various concentrations of oryzalin.

Combined imaging of cellulose synthase and microtubules using GFP-CESA3 [22] and mCherry-TUA5 [16] in growing leaves revealed both microtubule-associated CSCs (MCs) and ACs (Figure 1A). Overnight treatment with intermediate concentrations of oryzalin (3.2–6.4 μM) led to large enough gaps between microtubules for both ACs and MCs to be tracked over prolonged periods (Figures 1B–1D; Video S1). These intermediate concentrations did not affect the velocity of CSCs (Figure 1E), although higher concentrations have been shown to slow them down [23]. Both plus-end growth rates and minus-end shrink rates of microtubules were reduced approximately fourfold (Figures 1F–1G). The plus-end shrink rate following catastrophe or severing was approximately halved (Figure 1H). These findings are consistent with intermediate concentrations of oryzalin slowing down microtubule dynamics [24]. Oryzalin is thought to act by binding to the alpha subunit of the tubulin dimer to inhibit plus-end growth [25]. However, both minus-end shrink

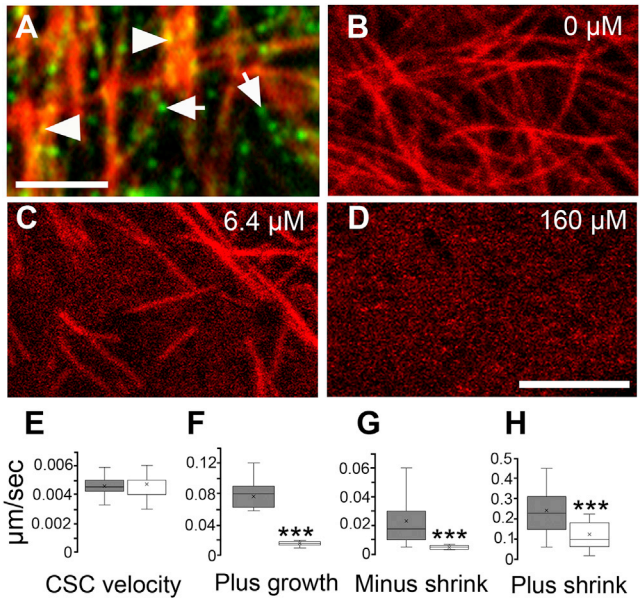


**Figure 1. Influence of Different Concentrations of Oryzalin on Microtubules**

(A) Localization of CSCs in an untreated leaf cell. MCs (arrow heads) lie directly over microtubules, and ACs (arrows) in the gaps between microtubules. mCherry-TUA5 (red: microtubules) and GFP-CESA3 (green: CSCs).

(B–D) Microtubule distributions in cells exposed to 0 μM (B), 6.4 μM (C), and 160 μM (D) oryzalin.

(E–H) Whisker boxplots of CSC and microtubule measurements in the absence (gray box) and presence (white box) of 6.4 μM oryzalin (x = mean). (E) Cellulose synthase velocity. Number of CSCs measured = 100 for each condition (in absence of oryzalin: median = 0.0045, mean = 0.0046 μm/sec, stdev = 0.0006, 3 cells and 2 plants; oryzalin-treated: median = 0.005, mean = 0.0047 μm/sec, stdev = 0.0008, 6 cells and 2 plants). (F) Plus-end growth rate. Number of plus ends measured = 24 (in absence of oryzalin: median = 0.08, mean = 0.08 μm/sec, stdev = 0.03, 3 cells and 2 plants; oryzalin-treated: median = 0.02, mean = 0.02 μm/sec, stdev = 0.003, 6 cells and 2 plants). (G) Minus-end shrink rate. Number of minus ends measured = 16 (in absence of oryzalin: median = 0.018, mean = 0.02 μm/sec, stdev = 0.02, 3 cells and 2 plants; oryzalin-treated: median = 0.005, mean = 0.005 μm/sec, stdev = 0.001, 6 cells and 2 plants). (H) Plus-end shrink rate. Number of plus ends measured = 31 (in absence of oryzalin: median = 0.23, mean = 0.24 μm/sec, stdev = 0.12, 6 cells and 2 plants; oryzalin-treated: median = 0.10, mean = 0.13 μm/sec, stdev = 0.09, 6 cells and 2 plants).

Asterisks mark distributions that are significantly different in the presence of intermediate oryzalin ($p < 0.00001$, Mann-Whitney U test). Bar, 5 μm in (A); 4 μm in (D). See also Video S1.

rate and plus-end growth rate are reduced, suggesting that oryzalin interferes with overall microtubule dynamics.

We used intermediate oryzalin treatments to monitor AC behavior. AC lifespan was 8.2 min (SD = 3.5; n = 162), similar to the lifespan reported for CSCs [20]. ACs spontaneously appeared in gaps between microtubules, as previously documented [16, 20]. In about half of the cases (57/106), after their appearance in a gap, ACs moved in a straight line until they disappeared or encountered a microtubule. In the remaining cases, ACs initially moved in a straight line but then changed trajectory while still in the gap (Figure 2A; Video S1). The turning angle varied from 10°–90° (Figure 2B), and the age of the AC at the time of turning also varied (Figure 2C). After turning, ACs sometimes turned a second (n = 5) or third time (n = 3). Taken together, these findings indicate that factors extrinsic to ACs, which cannot be microtubules, are guiding them.

A candidate extrinsic factor is the trail left by recently passing ACs (AC-trail). To test this hypothesis, we examined the history of AC trajectories in the vicinity of 55 cases where an AC had shown a sharp turn. In 20 cases (~35%), the AC turned to follow an AC-trail it encountered (Figures 2D–2F; Video S1); for 11 of these cases, ACs were redirected by trails running toward them, while 9 followed trails running away. In one of the 20 cases, the AC crossed over an extant trail prior to interaction, indicating that ACs can crossover other AC-trails but at a low frequency. Turns occurred at a mean of 4 min (328 s; SD = 257) after the trail-laying AC had passed (Figure 2G). The longest delay since the AC had passed was 19 min. In the remaining 35 cases, the turning AC did not encounter a recorded AC-trail within the period of time-lapse imaging (~40 min). It is possible that they encountered AC-trails left before the imaging began. The stability of the AC-trail turning cue (>19 min) is consistent with it being the cellulose microfibril synthesized by the trail-laying AC.

ACs could appear spontaneously along trails left by other ACs (16 appearances were observed along the 55 trails; Figure 2H). In 11 cases, newly appearing ACs moved along the previous AC-trails in either direction, whereas in the remaining 5 cases, they immediately left the trail (Videos S1 and S2). ACs occasionally disappeared on encounter with previous AC-trails (Video S2). Thus, AC-trails induce a range of behaviors: the turning of encountering ACs to join the trail, spontaneous appearances of new ACs that follow the trail, and disappearances of encountering ACs. Redirection of ACs may be caused by ACs colliding with nascent microfibrils (Figures 2I–2J). Axial appearance indicates nascent microfibrils may provide cues that promote insertion of CSCs.

## Cellulose Synthase Trajectories Reorient in the Absence of Microtubules and Are Sensitive to Cell Wall Structure

To determine how a population of ACs behaves in the absence of microtubules, seedlings expressing GFP-CESA3 and mCherry-TUA5 were exposed to high concentrations of oryzalin (160 μM; Figure 1D). Imaging of ACs started after all microtubules had disappeared (1 h; Figures 2K and 2N). The dominant alignment of AC trajectories persisted for many hours after microtubule removal (17 h; Figures 2L and O). However, over longer periods, the dominant alignment could change, sometimes shifting from a longitudinal to oblique or transverse (43 h, 5 cells; Figures 2M and 2P) or from oblique/transverse toward longitudinal (n = 5 cells). Thus, ACs can maintain alignments over many hours and also change alignment over longer time periods, most likely through interactions with nascent cellulose microfibrils.

If AC trajectories depend on microfibrils, they might be sensitive to enzymatic degradation of the cell wall. The effect of disrupting wall integrity on microtubule alignments has previously been evaluated using partial degradation with R10 cellulase [26], which includes both exoglucanases and endoglucanases [27]. Endoglucanase treatments can promote randomized wall architecture in cellulose-xyloglycan composites [28, 29].

Incubation of growing leaf cells with both R10 cellulase and high concentrations of oryzalin led to cells swelling after

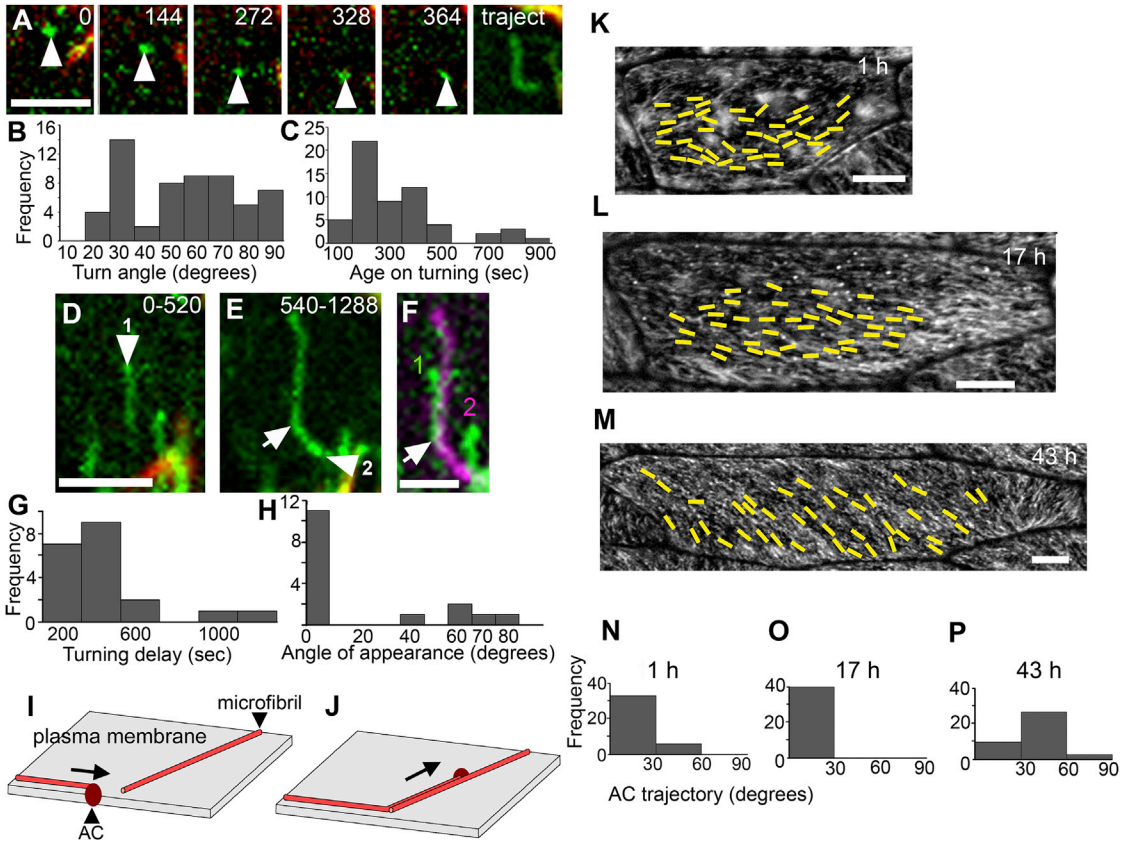


**Figure 2. Trajectories of ACs in Cells Treated with Intermediate Oryzalin**

(A) Video frames tracking an AC (arrowhead) after its first appearance. The time projection (traject) reveals the L-shaped trajectory.

(B) Histogram showing turning angles of ACs (n = 58, 7 cells and 2 plants).

(C) Histogram showing age of AC at time of turning (n = 58, 7 cells and 2 plants).

(D–F) Time projections showing an AC follow the trail left by a previous AC. (D) Arrowhead 1 shows the trail left by the first AC (AC1, the arrowhead also indicates its direction of movement). (E) Arrowhead 2 shows the trajectory of a subsequent AC (AC2) that turns spontaneously (arrow shows turning point). (F) Superimposing the trajectories in different colors (AC1 = green; AC2 = magenta) shows that AC2 turned to follow the trail left by AC1. The time interval covered by each projection is shown in seconds.

(G) Histogram showing how long ago the trail-laying AC passed at the time of turning (n = 58, 7 cells and 2 plants).

(H) Angles between trajectory of ACs and previous AC-trails on which they emerged (i.e., 0° = the newly emerging AC follows the trail) (n = 20, 7 cells and 2 plants).

(I and J) Model for the redirection of ACs based on interactions with cellulose microfibrils. (I) AC approaches obstructing cellulose microfibril. (J) AC redirects along the trajectory of the obstructing microfibril. Arrows indicate AC's direction of movement.

(K–M), Time projections showing the orientation of ACs trajectories (yellow lines) in a cell treated with 160 μM oryzalin at 1 (K), 17 (L), and 43 (M) h after removal of microtubules. Each time projection covers 200 s.

(N–P) Quantification of the AC-trajectories shown in (K–M) at 1 (K), 17 (L), and 43 (M) h after removal of microtubules. The trajectories were measured relative to the cell's long axis (i.e., bin 0°–30° corresponds to microtubules aligned with the cell's long axis).

Bar, 2 μm in (A), (D), and (E); 1 μm in (F); 5 μm in (I–K). See also Videos S1 and S2; Figure S1.

2–3 days. AC trajectories became less aligned, consistent with disruption of cell wall integrity influencing AC guidance (Figure S1; Video S2). However, ACs still exhibited turning (arrows; Figures S1A and S1C), indicating that the cellulase treatment did not completely remove obstructing microfibrils.

It has been suggested that microfibrils can be aligned by binding to scaffold proteins or polysaccharides located in the cell wall matrix [30]. The energy of binding is proposed to rotate nascent microfibrils to align with the scaffold. Our results suggest an alternative alignment mechanism: ACs are oriented by collision with microfibrils in the wall. Disrupting the arrangement of these microfibrils with R10 cellulase would then cause AC trajectories to be less organized.

The effect of R10 cellulase treatment on AC trajectories contrasts with its lack of effect on microtubule organization [26]. Microtubule alignment is, however, sensitive to mutations or drugs that inhibit cellulose synthesis [26]. Taken together with our findings, these results suggest MCs play a role in stabilizing microtubules, whereas feedback from the cell wall operates via ACs, which do not influence microtubule dynamics.

## The Autonomous Mechanism Is Overridden by the Microtubule Guidance System

To explore how these two guidance systems interact, we analyzed transitions between ACs and MCs at intermediate oryzalin concentrations. MCs could spontaneously appear either

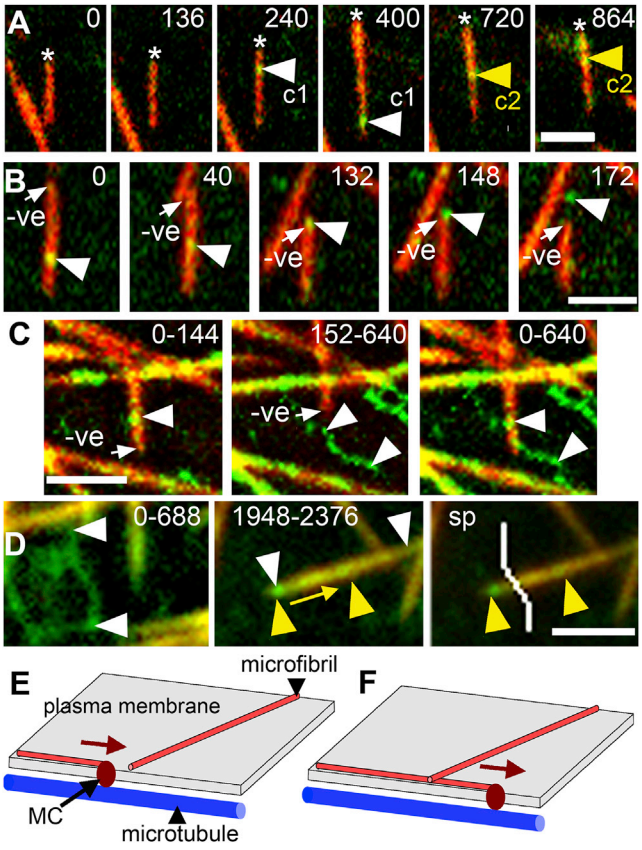


**Figure 3. Transitions of MCs to ACs and ACs to MCs**

(A) Video frames following the trajectories of two MCs appearing on a single microtubule. The asterisk marks the plus end of the young branch (which reaches cell edge at time 400). The first MC (white arrowhead) moves toward the minus end, whereas the second MC (yellow arrowhead) moves toward the plus end. mCherry-TUA5 (red: microtubules) and GFP-CESA3 (green: CSCs).

(B) Video frames showing an MC (arrowhead) drop off the microtubule's minus end and then continue moving in the same trajectory. The arrow (-ve) marks the shrinking minus end of the microtubule.

(C) Time projections showing an MC change trajectory after dropping off the minus end. The arrow head in projection 0–144 s marks the transition to an AC. The arrow heads in projection 152–640 s mark the skewed trajectory of the AC. Projection 0–640 s shows the movement of the CSC over the entire period.

(D) Time projections showing a microtubule and MC cross over a previous AC-trail. The arrowheads in projection 0–688 s show the trail left by an AC. The arrow heads in projection 1,948–2,376 s show the trajectory of microtubule with MC. Yellow arrowheads mark the trajectory of the MC along direction indicated by yellow arrow. Superimposing (SP) their trajectories shows that the microtubule and MC cross the trail of the previous AC (white line).

(E and F) Model for MCs ignoring microfibrils. (E) MC approaches obstructing cellulose microfibril. (F) MC passes beneath the obstructing microfibril. Brown arrows indicate MC's direction of movement.

Bar, 2 μm. See also Figures S2 and S3; Videos S1–S4.

on bundled microtubules, as previously described in [1], or on recently born single microtubules (single status was verified by kymographs) (Figures 3A, S2A, and S2B; Video S2). By following 50 MC appearances on single microtubules, we found 33 MCs went toward the microtubule minus end, while the other 17 traveled toward the plus end. MCs moving toward the minus end typically reached the microtubule end and dropped off, causing an MC-to-AC transition (Figure 3B; Video S3). The resulting ACs continued with their trajectories for a period but then exhibited turns, similar to that described above for spontaneously appearing ACs (Figure 3C; Video S3). Analysis of 50 MCs that dropped off minus ends showed that 23 (46%) displayed a turn, similar to the proportion 49/106 (46%) for spontaneously forming ACs (see above). Thus, when MCs transition to ACs, they behave in a similar way to spontaneously forming ACs.

By contrast, plus-end directed MCs remained associated with microtubules; MC translocation velocity was below that needed to catch up with plus-end growth. Thus, MCs can transition to ACs by exiting the minus ends of microtubules, and the resulting AC can maintain the microtubule trajectory for a limited period.

To follow the opposite transition, we analyzed the fate of ACs after encountering microtubules. Tracking 81 encounters revealed two types of interaction. In half of the cases (41), the AC disappeared upon microtubule encounter (Figure S3A; Video S3). In the other half, ACs were redirected along the microtubule to form MCs (Figure S3B; Video S3). Redirection could occur with single or bundled microtubules, and accounted for ~30% of MCs on single microtubules (22 redirections versus 54 spontaneous MC appearances). The type of AC-microtubule interaction was not dependent on the angle of encounter (Figure S3C). Thus, ACs disappear or switch to MCs upon encounter with microtubules—the interaction type may depend on the presence of CSI-1/POM1 bound to them [2, 17]. In three of the 81 encounters, ACs crossed over a different microtubule before the encounter. The failure to interact with the previous microtubule may reflect its deeper location in the cytoplasm [31].

To determine whether the redirection by microtubules overrides, or is overridden by, the autonomous system, we followed the fate of MCs encountering AC-trails. Tracking 12 of these encounters showed that MCs did not change trajectory or disappear when encountering AC-trails (Figures 3D, S2C, and S2D; Video S4), suggesting that the affinity of CSCs to microtubules can overcome the barrier created by nascent microfibrils (Figures 3E and 3F). Thus, the microtubule guidance system takes precedence over the autonomous system.

The dominance of the microtubule guidance system is also consistent with observed reorientation dynamics. Normally, microtubules and CSC trajectories are coaligned and reorient at a similar rate (within 1 h; [1, 22]; Figure S4A). In the absence of microtubules, ACs take an order of magnitude longer to reorient (~20 h). The difference in timescale suggests that microtubules normally drive reorientation of CSCs. To test this hypothesis, we filmed the behaviors of CSCs and microtubules before and after the addition of oryzalin. As predicted, CSCs stopped exhibiting rapid (hour-timescale) reorientations after microtubules disappeared (Figure S4B).

The mechanisms driving reorientations for the microtubule and autonomous systems are unclear. Reorientation behavior may reflect polymer dynamics (e.g., initiation at divergent trajectories and redirection or disappearance upon the encounter with other polymer molecules). The parameters for these interactions likely differ for the two systems, perhaps accounting for their distinct timescales. Computational modeling of reorienting behaviors, along the lines developed for studying cellulose synthase [32, 33] and microtubule dynamics [34, 35], may help clarify possible mechanisms.

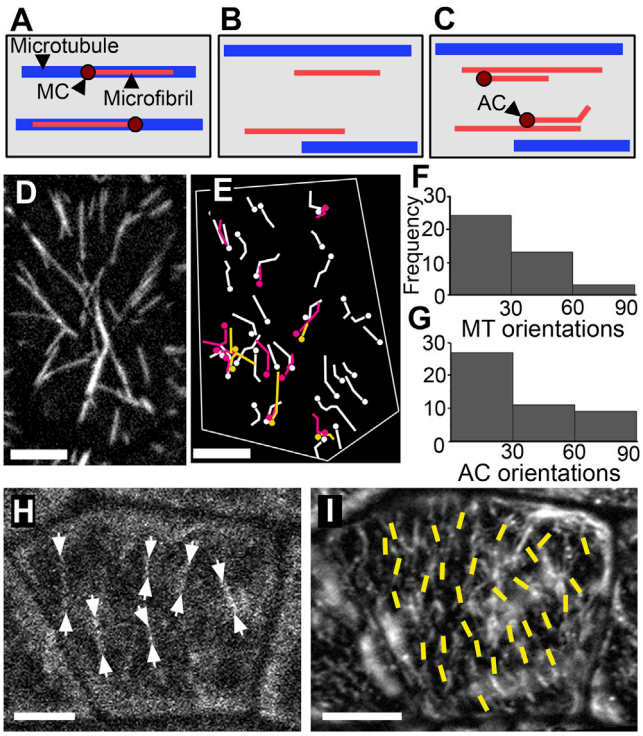


**Figure 4. Microtubules Indirectly Guide ACs**

(A–C) Cartoon illustrating the hypothesis for indirect guidance of ACs by microtubules, looking down on the plasma membrane (gray). (A) Microtubules guide MCs to deposit a corresponding alignment of nascent cellulose microfibrils in the cell wall. (B) Microfibrils remain after the guiding microtubules and MCs have gone (other microtubules also appear). (C) Microfibrils guide ACs to follow them in a similar alignment.

(D–G) Trajectories of microtubules and newly appearing ACs in cell treated with intermediate (6.4 μM) oryzalin. Orientations of microtubules (D) and the corresponding time projection showing the trajectories of ACs (E). The starts of trajectories are indicated by dots, colors indicate overlapping trajectories. (F and G) The orientations of microtubules and AC trajectories shown in (D) and (E), respectively, measured relative to the cell's long axis (0°). The distribution of AC orientations is not significantly different from the distribution of microtubule orientations ($p = 0.44$, chi square = 1.7, 2 degrees of freedom). The distribution of the AC orientations is significantly different from a uniform distribution where there is an equal chance of emerging at any angle ($p = 0.034$, chi square = 6.7, 2 degrees of freedom). AC trajectories were tracked over a 40 min interval.

(H and I) Memory of main microtubule orientation in cells treated with high (160 μM) oryzalin. (H) Image of microtubules just before they disappeared. The arrow heads mark the ends of microtubules. (I) The corresponding time projection taken ~1 h after microtubules had gone, showing AC trajectories (yellow lines). Trajectories were tracked over a ~3 min period, n = 30.

Bar, 5 μm in (D), (E), and (H); 4 μm in (I). See also Figure S4; Video S4.

## Microtubules Can Indirectly Guide ACs

By guiding MCs, microtubules should promote a corresponding alignment of nascent microfibrils in the cell wall (Figures 4A and 4B). These nascent microfibrils will in turn guide ACs, generating more nascent microfibrils that further promote the same alignment (Figure 4C). Consistent with this hypothesis, we found that MC trails could cause encountering ACs to turn to follow them (Video S4). Thus, MCs can guide ACs indirectly via nascent microfibril trails.

Such a mechanism would predict that spontaneously arising ACs would tend to follow the dominant alignment of microtubules. To test this hypothesis, we tracked the trajectories of newly emerging ACs in cells treated with intermediate concentrations of oryzalin. Plotting AC trajectories revealed that they aligned with the dominant microtubule orientation (Figures 4D–4G and S4C–S4F). These findings are thus consistent with microtubules indirectly guiding ACs.

A further prediction of indirect guidance is that ACs may perpetuate microtubule orientations after microtubules have disappeared. To test this prediction, we treated cells with high oryzalin concentrations (160 μM) and imaged microtubules just before they disappeared. All cells (8/8) displayed AC trajectory orientations similar to those of the last microtubule alignment ~1 h after microtubule disappearance (Figures 4H, 4I, S4G, and S4H). Given the CSC turnover rate of approximately 7–8 min ([20] and our measurements), most of these ACs would not have directly experienced microtubule guidance. The proportion of cells showing AC trajectories similar to the last microtubule alignment decreased to ~72% (16/22) and then ~33% (6/18) of cells after 18 and 42 h, respectively. None of the 6 cells observed after 62 h displayed alignments matching the last dominant microtubule orientation. Thus, a memory of microtubule orientation is maintained, likely via the template of microfibrils in the cell wall for several hours, and is then gradually lost.

Such a memory system may also be involved in maintaining secondary wall patterns during xylem vessels development. Establishing the pattern of secondary wall microfibrils requires microtubules, but the pattern can then be maintained in their absence [36]. It was hypothesized that this maintenance may be because of membrane-based guidance, restriction of Golgi movement, or guidance by cell wall polymers. Our findings are consistent with the latter hypothesis, with microfibrils providing the guidance. Other candidate guidance polymers are xylan and lignin which colocalize with microfibrils [37]. However, rather than maintain organized patterns, xylan and lignin become disorganized when microtubules are removed in a CESA mutant (*baculites*). Thus, their organization depends on both CESA and microtubules, making it unlikely that they provide an independent guidance system.

## Role of Autonomous and Microtubule Guidance Systems

Given the ability of the autonomous system to maintain aligned CSC trajectories, what is the biological role of microtubule guidance? While the autonomous system can maintain CSC alignments, its dependence on prior wall texture may render it difficult to control through developmental or environmental cues. The main role of the dominant microtubule guidance system may therefore be to provide such control by allowing a rapid and flexible mechanism for controlling cellulose microfibrils alignments that is less constrained by prior wall architecture [38–40].

The dual guidance behavior we describe is akin to a model for cell wall synthesis in rod-shaped bacteria, where it has been proposed that cell wall synthesis complexes create a tail of peptidoglycan that provide a template to guide other cell wall synthesis complexes [8]. As with the plant cell wall, two guidance mechanisms are at play: one dependent on interaction

with nascent wall fibers, the other on the cytoskeleton (actin homolog MreB, playing the equivalent role of microtubules). Having dual guidance may therefore provide a general mechanism to ensure both strong coherence and flexibility of response, allowing effective regulation of the growth and strength of cell walls.

## STAR★METHODS

Detailed methods are provided in the online version of this paper and include the following:

- KEY RESOURCES TABLE
- LEAD CONTACT AND MATERIALS AVAILABILITY
- EXPERIMENTAL MODEL AND SUBJECT DETAILS
  - Growth conditions
- METHOD DETAILS
  - Microscopy
  - Image processing
- QUANTIFICATION AND STATISTICAL ANALYSIS
- DATA AND CODE AVAILABILITY

### SUPPLEMENTAL INFORMATION

Supplemental Information can be found online at https://doi.org/10.1016/j.cub.2019.12.066.

### ACKNOWLEDGMENTS

We thank Grant Calder, Eva Wegel, and the JIC BioImaging facility for help with TIRF microscopy. We also thank Desmond Bradley and the other members of the Coen lab for useful discussions about this paper. Finally, we thank JIC Horticultural services. The work was supported by grants from the UK Biotechnology and Biological Sciences Research Council (BB/L008920/1, BBS/E/J/00000152, BB/F005997/1, and BBS/E/J/000PR9787).

### AUTHOR CONTRIBUTIONS

J.C. and E.C. conceived and designed the study. J.C. acquired data and developed resources. J.C. analyzed the data. J.C. and E.C. interpreted the data. E.C. provided supervision. J.C. and E.C. wrote the manuscript. All authors reviewed and revised the manuscript.

### DECLARATION OF INTERESTS

The authors declare no competing interests.

Received: July 4, 2019
Revised: November 14, 2019
Accepted: December 19, 2019
Published: February 6, 2020

### REFERENCES

1. Paredez, A.R., Somerville, C., and Ehrhardt, D. (2006). Visualization of cellulose synthase demonstrates functional association with microtubules. Science *312*, 1491–1495.
2. Bringmann, M., Li, E., Sampathkumar, A., Kocabek, T., Hauser, M.-T., and Persson, S. (2012). POM-POM2/cellulose synthase interacting1 is essential for the functional association of cellulose synthase and microtubules in Arabidopsis. Plant Cell *24*, 163–177.
3. Lei, L., Li, S., and Gu, Y. (2012). Cellulose synthase interactive protein 1 (CSI1) mediates the intimate relationship between cellulose microfibrils and cortical microtubules. Plant Signal. Behav. *7*, 714–718.
4. Liu, Z., Schneider, R., Kesten, C., Zhang, Y., Somssich, M., Zhang, Y., Fernie, A.R., and Persson, S. (2016). Cellulose-Microtubule Uncoupling Proteins Prevent Lateral Displacement of Microtubules during Cellulose Synthesis in Arabidopsis. Dev. Cell *38*, 305–315.
5. Sugimoto, K., Himmelspach, R., Williamson, R.E., and Wasteneys, G.O. (2003). Mutation or drug-dependent microtubule disruption causes radial swelling without altering parallel cellulose microfibril deposition in Arabidopsis root cells. Plant Cell *15*, 1414–1429.
6. Himmelspach, R., Williamson, R.E., and Wasteneys, G.O. (2003). Cellulose microfibril alignment recovers from DCB-induced disruption despite microtubule disorganization. Plant J. *36*, 565–575.
7. Shi, H., Bratton, B.P., Gitai, Z., and Huang, K.C. (2018). How to Build a Bacterial Cell: MreB as the Foreman of E. coli Construction. Cell *172*, 1294–1305.
8. Zhao, H., Patel, V., Helmann, J.D., and Dörr, T. (2017). Don't let sleeping dogmas lie: new views of peptidoglycan synthesis and its regulation. Mol. Microbiol. *106*, 847–860.
9. Ghazanfari, S., Khademhosseini, A., and Smit, T.H. (2016). Mechanisms of lamellar collagen formation in connective tissues. Biomaterials *97*, 74–84.
10. Yamamoto, T., Hasegawa, T., Hongo, H., and Amizuka, N. (2019). Alternating lamellar structure in human cellular cementum and rat compact bone: Its structure and formation. J Oral Biosci. *61*, 105–114.
11. Emons, A.M.C., Höfte, H., and Mulder, B.M. (2007). Microtubules and cellulose microfibrils: how intimate is their relationship? Trends Plant Sci. *12*, 279–281.
12. Zhang, T., Zheng, Y., and Cosgrove, D.J. (2016). Spatial organization of cellulose microfibrils and matrix polysaccharides in primary plant cell walls as imaged by multichannel atomic force microscopy. Plant J. *85*, 179–192.
13. Satiat-Jeunemaitre, B., Martin, B., and Hawes, C. (1992). Plant cell wall architecture is revealed by rapid-freezing and deep-etching. Protoplasma *167*, 33–42.
14. McFarlane, H.E., Döring, A., and Persson, S. (2014). The cell biology of cellulose synthesis. Annu. Rev. Plant Biol. *65*, 69–94.
15. Somerville, C. (2006). Cellulose synthesis in higher plants. Annu. Rev. Cell Dev. Biol. *22*, 53–78.
16. Gutierrez, R., Lindeboom, J.J., Paredez, A.R., Emons, A.M.C., and Ehrhardt, D.W. (2009). Arabidopsis cortical microtubules position cellulose synthase delivery to the plasma membrane and interact with cellulose synthase trafficking compartments. Nat. Cell Biol. *11*, 797–806.
17. Li, S., Lei, L., Somerville, C.R., and Gu, Y. (2012). Cellulose synthase interactive protein 1 (CSI1) links microtubules and cellulose synthase complexes. Proc. Natl. Acad. Sci. USA *109*, 185–190.
18. Fujita, M., Himmelspach, R., Hocart, C.H., Williamson, R.E., Mansfield, S.D., and Wasteneys, G.O. (2011). Cortical microtubules optimize cell-wall crystallinity to drive unidirectional growth in Arabidopsis. Plant J. *66*, 915–928.
19. Giddings, T.H., Jr., and Staehelin, L.A. (1988). Spatial relationship between microtubules and plasma-membrane rosettes during the deposition of primary wall microfibrils in Closterium sp. Planta *173*, 22–30.
20. Sampathkumar, A., Gutierrez, R., McFarlane, H.E., Bringmann, M., Lindeboom, J., Emons, A.-M., Samuels, L., Ketelaar, T., Ehrhardt, D.W., and Persson, S. (2013). Patterning and lifetime of plasma membrane-localized cellulose synthase is dependent on actin organization in Arabidopsis interphase cells. Plant Physiol. *162*, 675–688.
21. Emons, A.M.C., and Mulder, B.M. (1998). The making of the architecture of the plant cell wall: how cells exploit geometry. Proc. Natl. Acad. Sci. USA *95*, 7215–7219.
22. Chan, J., Crowell, E., Eder, M., Calder, G., Bunnewell, S., Findlay, K., Vernhettes, S., Höfte, H., and Lloyd, C. (2010). The rotation of cellulose synthase trajectories is microtubule dependent and influences the texture of epidermal cell walls in Arabidopsis hypocotyls. J. Cell Sci. *123*, 3490–3495.

23. Woodley, M., Mulvihill, A., Fujita, M., and Wasteneys, G.O. (2018). Exploring Microtubule-Dependent Cellulose-Synthase-Complex Movement with High Precision Particle Tracking. Plants (Basel) *7*, E53.
24. Nakamura, M., Naoi, K., Shoji, T., and Hashimoto, T. (2004). Low concentrations of propyzamide and oryzalin alter microtubule dynamics in Arabidopsis epidermal cells. Plant Cell Physiol. *45*, 1330–1334.
25. Hugdahl, J.D., and Morejohn, L.C. (1993). Rapid and Reversible High-Affinity Binding of the Dinitroaniline Herbicide Oryzalin to Tubulin from Zea mays L. Plant Physiol. *102*, 725–740.
26. Paredez, A.R., Persson, S., Ehrhardt, D.W., and Somerville, C.R. (2008). Genetic evidence that cellulose synthase activity influences microtubule cortical array organization. Plant Physiol. *147*, 1723–1734.
27. Beldman, G., Searle-Van Leeuwen, M.F., Rombouts, F.M., and Voragen, F.G. (1985). The cellulase of Trichoderma viride. Purification, characterization and comparison of all detectable endoglucanases, exoglucanases and β-glucosidases. Eur J Biochem. *146*, 301–308.
28. Chanliaud, E., Silva, J., De, Strongitharm, B., Jeronimidis, G., and Gidley, M.J. (2004). Mechanical effects of plant cell wall enzymes on cellulose/xyloglucan composites. Plant J. *38*, 27–37.
29. Whitney, S.E., Brigham, J.E., Darke, A.H., Reid, J.G., and Gidley, M.J.G. (1995). In vitro assembly of cellulose / xyloglucan networks : ultrastructural and molecular aspects. Plant J. *8*, 491–504.
30. Baskin, T.I. (2001). On the alignment of cellulose microfibrils by cortical microtubules: a review and a model. Protoplasma *215*, 150–171.
31. Barton, D.A., Vantard, M., and Overall, R.L. (2008). Analysis of cortical arrays from Tradescantia virginiana at high resolution reveals discrete microtubule subpopulations and demonstrates that confocal images of arrays can be misleading. Plant Cell *20*, 982–994.
32. Diotallevi, F., and Mulder, B. (2007). The cellulose synthase complex: a polymerization driven supramolecular motor. Biophys. J. *92*, 2666–2673.
33. Haigler, C.H., Grimson, M.J., Gervais, J., Le Moigne, N., Höfte, H., Monasse, B., and Navard, P. (2014). Molecular modeling and imaging of initial stages of cellulose fibril assembly: evidence for a disordered intermediate stage. PLoS ONE *9*, e93981.
34. Tindemans, S.H., Hawkins, R.J., and Mulder, B.M. (2010). Survival of the aligned: ordering of the plant cortical microtubule array. Phys. Rev. Lett. *104*, 058103.
35. Allard, J.F., Wasteneys, G.O., and Cytrynbaum, E.N. (2010). Mechanisms of self-organization of cortical microtubules in plants revealed by computational simulations. Mol. Biol. Cell *21*, 278–286.
36. Schneider, R., Tang, L., Lampugnani, E.R., Barkwill, S., Lathe, R., Zhang, Y., McFarlane, H.E., Pesquet, E., Niittyla, T., Mansfield, S.D., et al. (2017). Two Complementary Mechanisms Underpin Cell Wall Patterning during Xylem Vessel Development. Plant Cell *29*, 2433–2449.
37. Takenaka, Y., Watanabe, Y., Schuetz, M., Unda, F., Hill, J.L., Jr., Phookaew, P., Yoneda, A., Mansfield, S.D., Samuels, L., Ohtani, M., and Demura, T. (2018). Patterned Deposition of Xylan and Lignin is Independent from that of the Secondary Wall Cellulose of Arabidopsis Xylem Vessels. Plant Cell *30*, 2663–2676.
38. Chan, J., Calder, G., Fox, S., and Lloyd, C. (2007). Cortical microtubule arrays undergo rotary movements in Arabidopsis hypocotyl epidermal cells. Nat. Cell Biol. *9*, 171–175.
39. Hamant, O., Heisler, M.G., Jönsson, H., Krupinski, P., Uyttewaal, M., Bokov, P., Corson, F., Sahlin, P., Boudaoud, A., Meyerowitz, E.M., et al. (2008). Developmental patterning by mechanical signals in Arabidopsis. Science *322*, 1650–1655.
40. Lindeboom, J.J., Nakamura, M., Hibbel, A., Shundyak, K., Gutierrez, R., Ketelaar, T., Emons, A.M., Mulder, B.M., Kirik, V., and Ehrhardt, D.W. (2013). A mechanism for reorientation of cortical microtubule arrays driven by microtubule severing. Science *342*, 1245533.
41. Fonck, E., Feigl, G.G., Fasel, J., Sage, D., Unser, M., Rüfenacht, D.A., and Stergiopulos, N. (2009). Effect of aging on elastin functionality in human cerebral arteries. Stroke *40*, 2552–2556.
42. Calder, G., Hindle, C., Chan, J., and Shaw, P. (2015). An optical imaging chamber for viewing living plant cells and tissues at high resolution for extended periods. Plant Methods *11*, 22.

# STAR★METHODS

## KEY RESOURCES TABLE

| REAGENT or RESOURCE | SOURCE | IDENTIFIER |
|---|---|---|
| Chemicals, Peptides, and Recombinant Proteins | | |
| Oryzalin | Sigma-Aldridge | Cat#36182 |
| Cellulase "Onozuka" R-10 | Yakult Pharmaceutical, Japan | N/A |
| Experimental Models: Organisms/Strains | | |
| *Arabidopsis* plants containing GFP-CESA3 | [22] | Available on request |
| *Arabidopsis* plants containing mCherry-TUA5 | [16] | Available on request |
| F2 *Arabidopsis* plants containing GFP-CESA3 and mCherry-TUA5 | This paper | Available on request |
| Software and Algorithms | | |
| ImageJ | Freely available | ImageJ https://imagej.nih.gov/ij/ |
| OrientationJ Plugin for ImageJ | [41] | N/A |
| Mann-Whitney U tests | Freely available | https://www.socscistatistics.com/tests/mannwhitney/Default2.aspx. |
| Chi-square goodness of fit tests | Freely available | http://quantpsy.org/chisq/chisq.htm |

## LEAD CONTACT AND MATERIALS AVAILABILITY

Further information and requests for plant lines and raw data should be directed to and will be fulfilled by the corresponding author and Lead Contact, Jordi Chan (jordi.chan@jic.ac.uk) and Enrico Coen (enrico.coen@jic.ac.uk).

## EXPERIMENTAL MODEL AND SUBJECT DETAILS

*Arabidopsis thaliana* plants expressing GFP-CESA3 [22] were crossed with mCherry-TUA5 [16]. F2 seedlings were used for experiments.

### Growth conditions

Plants were grown on plates containing 1% (w/v) Agar, 1% (w/v) glucose, 0.43% (w/v) Murashige & Skoog powdered medium including vitamins, 3 mM MES, PH 5.7. Seeds were stratified at 4°C for 2 days and then germinated at 20°C under a 16 h light/8 h dark cycle. 5-6 day old seedlings were transferred from plates into a Bioimaging chamber [22, 42] containing 0.43% (w/v) Murashige & Skoog powdered medium including vitamins containing 1% (w/v) glucose, pH 5.8. The growth medium was replaced after a 1-2 day acclimation period with growth media containing either 160 μM or 6.4 μM oryzalin (Sigma-Aldridge, 36182) or 160 μM oryzalin and 2% (w/v) cellulase "Onozuka" R-10 (Yakult Pharmaceutical Ind, Japan). Note that although this cellulase preparation has high cellulase activity, it still contains hemicellulases, and it degrades mannans, xylans, galactomannans, pectins and other polysaccharides [27].

## METHOD DETAILS

### Microscopy

Near TIRF videos of leaf cells were collected using Zeis Elya PS1 microscope equipped with a 100 x/1.46 NA objective lens. GFP was excited using a 488 nm laser and the emitted light filtered through a 495-550 band pass filter. A 561 nm excitation laser and a BP575-640 nm emission filter were used for RFP imaging. GFP and RFP images were collected simultaneously. The TIRF angle was typically set at 65-68. Videos were acquired with an interval of 2-8 s.

Confocal microscopy of leaf cells was carried out using either a Zeis 780 or 880 confocal laser scanning microscope equipped with a x40/1.3 NA or x63/1.3 NA objective lens. A 488 nm laser and 495-550 band pass emission filter were used to image GFP. A 561 nm excitation laser and a BP570-620 nm emission filter were used for RFP imaging. Confocal sections were collected at a z-spacing of 0.2-4 μm and z stacks acquired with an interval of 4-8 s. For experiments carried out using high oryzalin concentrations (160 μM), microtubules (mCherry-TUA5) were imaged first until they disappeared (a z stack was collected every 15 min). Imaging of GFP-CESA3 (in addition to mCherry-TUA5) was then started ~1 or ~16 h after disappearance – depending on whether microtubule removal was carried out in the morning or overnight, respectively.

### Image processing

All processing was carried out using Fiji, a version of ImageJ. Tools included in this software were used to project z-data using maximum or sum projection, rotate, crop, align, reslice, adjust brightness and contrast, background subtract and add scale bars and time stamps to videos. Montages were assembled using Adobe Photoshop.

## QUANTIFICATION AND STATISTICAL ANALYSIS

Quantification of microtubules (i.e., plus-end growth and shrink rates, minus-end shrink rates) and cellulose synthase (i.e., velocity) were measured from kymographs projected along the trajectories of growing microtubules or moving CSCs using the Reslice tool of ImageJ. Rates were estimated from the slopes of the traces.

For experiments with intermediate (6.4 μM) oryzalin, microtubule and AC trajectories were measured relative to the cell's long axis. For experiments with high oryzalin (160 μM), mean microtubule orientations and AC trajectories were quantified from sum projections of z stacks (microtubule) or videos (GFP-CESA3) using the OrientationJ plugin [41]. Array orientations were classed as ether longitudinal, oblique or transverse if the mean angle was between 0-30°, 30-60° or 60-90° relative to the cell's long axis. Oblique arrays were further classed as either S- or Z-oblique depending on whether microtubule or CSC trajectories went from the top left to bottom right or top right to bottom left corners of the cell, respectively. To aid visualization, in some examples, AC trajectories were manually tracked and labeled.

Mann-Whitney U tests were performed at (https://www.socscistatistics.com/tests/mannwhitney/Default2.aspx.). Tests were performed using a significance level of 0.05, 2 tailed. Chi-square goodness of fit tests were performed at http://quantpsy.org/chisq/chisq.htm, using a significance level of 0.05, two degrees of freedom.

## DATA AND CODE AVAILABILITY

This study did not generate any unique code. Data are available at figshare:10.6084/m9.figshare.11406888.

**Current Biology, Volume *30***

## Supplemental Information

# Interaction between Autonomous and Microtubule Guidance Systems Controls Cellulose Synthase Trajectories

**Jordi Chan and Enrico Coen**

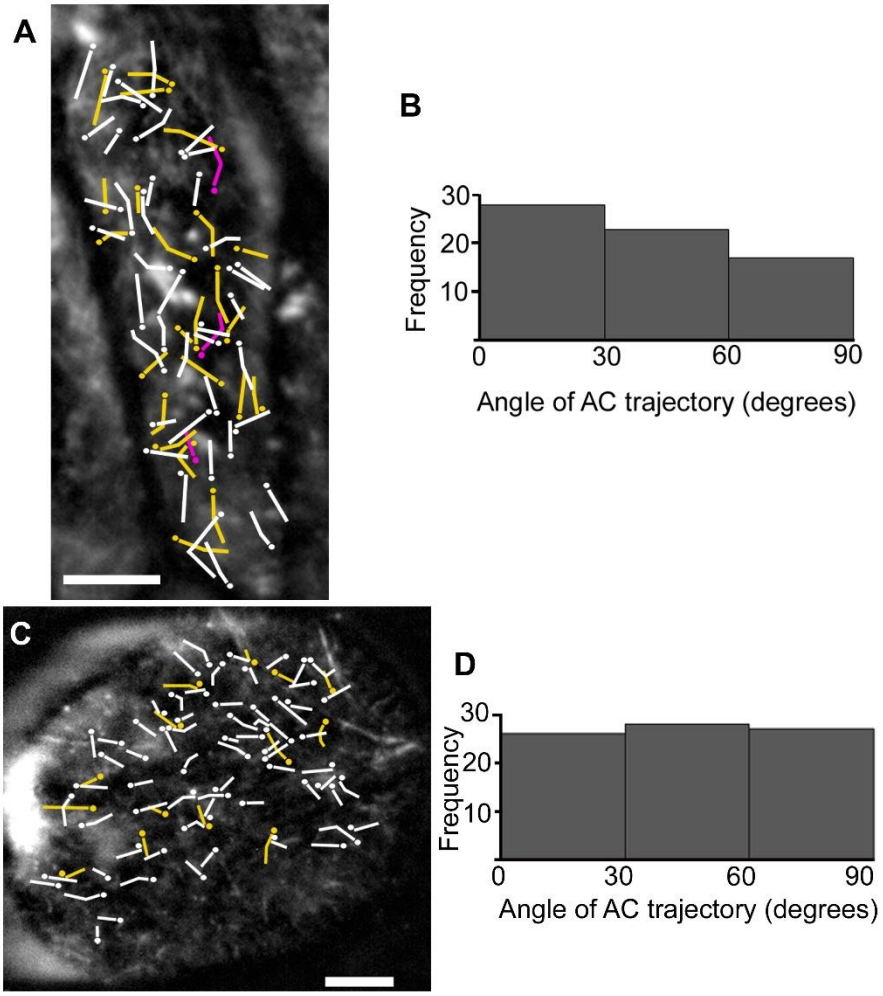


**Figure S1: AC trajectories in cells treated with oryzalin and cellulase. Related to Figure 2.**

(**A, C**) Time projections showing the trajectories of newly-appearing ACs after 2- and 3-days exposure to the drugs, respectively. Dots close to lines indicate the start of trajectories, colours indicate overlapping trajectories. (**B, D**) Histograms of the orientations of AC trajectories shown in panels A and B, respectively. The trajectories were measured relative to the cell's long axis. Bar = 5 µm. See also Video S2.

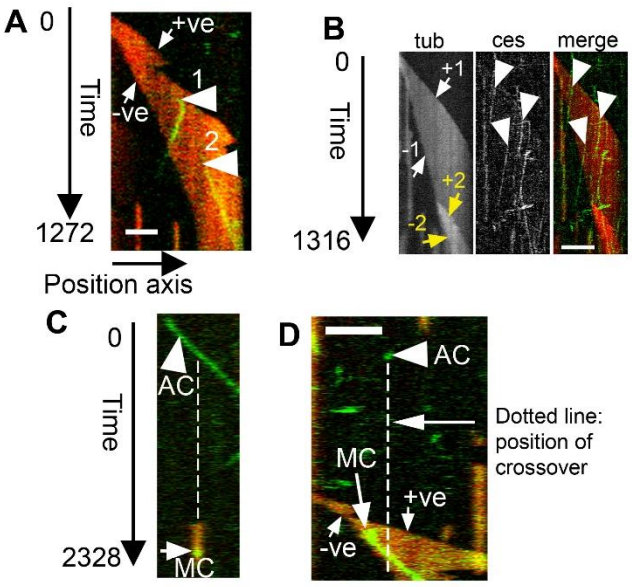


**Figure S2: Kymographs of MCs. Related to Figure 3.**

(**A**) Appearance of two MCs along a single microtubule. The kymograph was projected along the axis of the microtubule shown Figure 3A; The merge shows both imaging channels: mCherry-TUA5 (red: microtubules) and GFP-CESA3 (green: CSCs). The shape of the red trace is generated by the growth and shrinkage of the microtubule ends. The saw-tooth appearance of the leading edge is generated by phases of growth and shrinkage of the plus end (+ve). The sloping trace of the lagging edge is generated by the shrinkage of the minus end (-ve). The arrow heads mark the appearance of MCs. The orientations of the green sloping traces show that the two MCs move in opposite directions: MC1 moves towards the minus end, whereas MC2 moves towards the plus end (2). Note: the microtubule trace contains one plus (+ve) and one minus end (-ve) indicating that it is single. **(B**) Appearance of MCs before microtubule bundling. The microtubule trace illustrates key features of a single microtubule becoming bundled in parallel (tub). First, the appearance of additional plus and minus end traces (yellow arrows, +2, -2, respectively); and second, an increase in the intensity of fluorescence along the bundled portion due to the side-by-side arrangement of microtubules. Arrowheads mark the site of appearance of MCs which then travel towards the minus end of the microtubule. Note the MCs appeared before bundling took place (ces, merge). (**C-D**), Kymographs supporting Figure 3D showing a microtubule and MC crossing at approximately right angles over a trail left by an AC. (**C**) Kymograph projected along the AC trajectory, generating a sloping trace (arrowhead; AC). The crossing microtubule appears later and leaves a red vertical trace. The arrow (MC) indicates the trace generated by the crossing MC. (**D**) Kymograph projected along the axis of the crossing microtubule. The AC appears as a spot (arrowhead: ac) in orthogonal view. The red trace corresponds to the crossing microtubule. Edges generated from the plus and minus ends are marked +ve and -ve, respectively. The arrow (mc) marks the sloping trace of the MC. The dotted line indicates the position where microtubule and MC crossover the trail of the AC. Bar: A, C, D = 2 µm; B = 3 µm. Time = sec. See also Videos S2-S3.

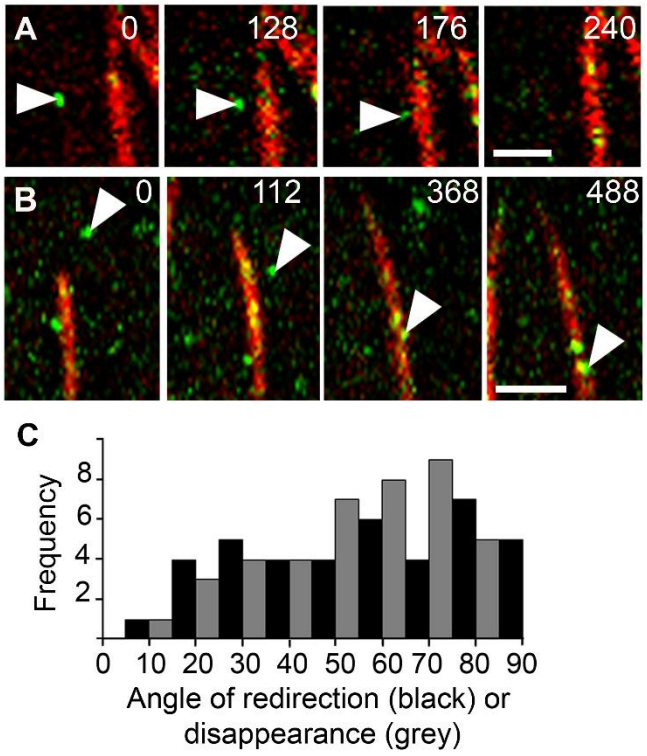


**Figure S3: AC interactions with microtubules. Related to Figure 3.**

(**A**) Video frames showing an AC (arrowhead) disappear on encountering a microtubule. (**B**) Video frames showing an AC (arrowhead) redirect on encountering a microtubule. (**C**) Frequency histogram showing angles of redirection (black bars) versus disappearance (grey bars). N= 81, 7 cells, 3 plants. Bar A = 0.75 µm; B = 2 µm, Time = sec. See also Video S3.

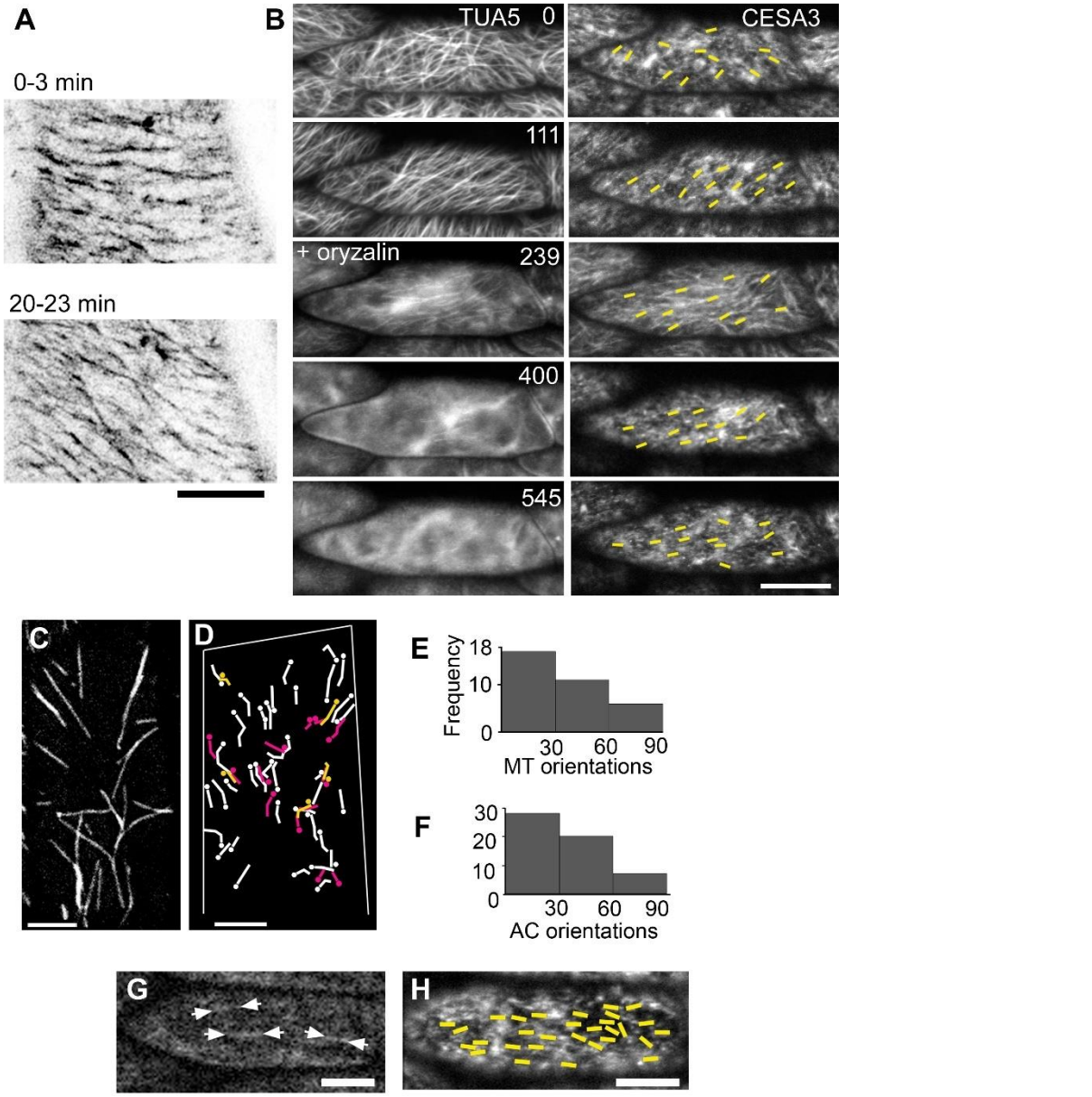


**Figure S4: CSC behaviour in cells exposed to different oryzalin concentrations. Related to Figure 4.**

(**A**) Time projections showing CSC trajectories change orientation in the absence of oryzalin. In this example, they changed from transverse (0-3 min) to oblique (20-23 min). Each image reflects the movement of CSCs over ~ 3 min period. (**B**) Time series showing the behaviour of CSCs in the presence and absence of 160 µM oryzalin. Before oryzalin was added, microtubule (TUA5) and CSC trajectories (CESA3) regularly changed orientation from mixed (0 min) to oblique (111 min) and were longitudinal when oryzalin was added at 239 min. CSC trajectories remained longitudinal when the cells were imaged 2 (400 min) and 4 hours (545 min) later when microtubule were gone. Yellow lines indicate CSC trajectories. The trajectories were marked from videos covering ~ 4 min period. (**C-H**) Microtubules indirectly guide ACs. Microtubule (C) and AC (D) trajectories are similar in a cell treated with 6.4 µM oryzalin. Dots close to lines indicate the start of trajectories, colours indicate overlapping trajectories. (**E-F**) Quantification of the orientations of microtubules and AC trajectories shown in panel C and D, respectively. The distribution of AC orientations is not significantly different from the distribution of microtubule orientations (p= 0.8, chi square = 0.4, 2 degrees of freedom).

The distribution of AC orientations is significantly different from a uniform distribution where there is an equal chance of emerging at any angle (p= 0.031, chi square = 7, 2 degrees of freedom). Trajectories were tracked over a 27 min interval, n=55. (**G-H**) AC trajectories reflect the orientations of the last microtubules in cell treated with 160 µM oryzalin. (**G**) Image of the microtubules before they disappeared. The last microtubules were parallel to the cell's long axis (arrow heads mark the ends of microtubules). (**H**) The corresponding time projection taken ~1 hour after microtubules had gone showing the orientations of AC trajectories (yellow lines) were also parallel to the cell's long axis. Trajectories were tracked over a period of ~3 min, n= 30. Bar: A =6 µm; B = 15 µm; C, D, H= 5 µm; G = 2.5 µm.